Molten Globule Monomer to Condensed Dimer: Role of Disulfide Bonds in Platelet Factor-4 Folding and Subunit Association†

Kevin H. Mayo* and Sharon Barker

Structural Biology Group, Jefferson Cancer Institute, Departments of Pharmacology and Biochemistry & Molecular Biology, Thomas Jefferson University, Philadelphia, Pennsylvania 19107

Michael J. Kuranda, Anthony J. Hunt, Jill A. Myers, and Theodore E. Maione

Repligen Corporation, One Kendall Square, Building 700, Cambridge, Massachusetts 02139

Received April 10, 1992; Revised Manuscript Received September 25, 1992

ABSTRACT: Platelet factor 4 (PF4) exhibits high affinity for heparin and exists as a tetramer in solution under physiologic conditions. Reduction of the two disulfide bridges in PF4 increases the protein's dissociation constant for heparin approximately 20-fold and shifts the highest apparent aggregation state from tetramer to dimer as evidenced by gel filtration, chemical cross-linking, and ^{1}H-NMR studies. ^{1}H-NMR spectra of reduced PF4 monomers generally show narrower, less dispersed, upfield-shifted NH and αH resonances, suggesting the presence of an unfolded monomer state. Reduced PF4 monomer folding, however, is evidenced by the presence of about 12 relatively long-lived backbone NHs and by CD spectra that indicate conservation of overall secondary structure. These data suggest the presence of a molten globule-type state. Urea denaturation shifts this apparent molten globule to a fully unfolded state characterized by more random coil-like resonance shifts. The reduced PF4 dimer state yields NMR and CD data consistent with preservation of tertiary structural folds found for the native species. In this regard, the reduced PF4 folding transition is thermodynamically linked with dimer formation which stabilizes tertiary structure. Monomer–dimer association equilibria for reduced PF4 essentially follow the same pH and salt titration trends as reported previously for native PF4 dimers [Mayo, K. H., & Chen, M. J. (1989) *Biochemistry 28*, 9469–9478], indicating that that dimer interface is generally conserved in the absence of disulfide constraints. Reduced PF4 tetramers are not apparent under any conditions investigated, suggesting that disulfides are necessary for efficient antiparallel β-sheet alignment between dimer pairs.

Protein folding is primarily dictated by noncovalent, relatively weak intramolecular forces [see review by Jaenicke (1991)]. Normally viewed as a highly cooperative process, folding has often been considered an "all or nothing" event. Only recently has considerable evidence been accumulated to indicate that folding of a protein into "native" conformation proceeds through various intermediate species (Jaenicke, 1991). Since the time scale of protein folding is generally on the order of seconds or less, studying such a partly folded transient intermediate state(s) and a folding pathway(s) generally requires the use of indirect methods like NMR proton/deuteron trapping (Udgaonkar & Baldwin, 1988; Roder et al., 1988; Bycroft et al., 1990), kinetic refolding of protein engineered mutants (Matouschek et al., 1990), or microcalorimetric thermodynamic dissection (Freire et al., 1992).

While most intermediates are highly transient, various ones can be stabilized at equilibrium by low pH (about pH 2), low ionic strength, or elevated temperature or in the presence of some denaturant. One of these stable intermediate species has been called the "molten globule" state (Ptitsyn, 1987; Kuwajima, 1989) which is a commonly envoked term for prefolded structures which possess a relatively more open conformation with increased solvent exposure of hydrophobic groups. In this state, there are elements of secondary structure, but few, if any, tertiary structural contacts. This partially condensed state, while not often observed, has been found for a number of proteins (Jaenicke, 1991). Investigation of such stable intermediates can provide useful information toward understanding protein folding. The first well-defined examples of molten globule states were those of α-lactalbumin and cytochrome *c* at acid pH (Dolgikh et al., 1981, 1983; Ohgushi & Wada, 1983). More detailed descriptions of molten globule states have been provided, for example, by NMR and optical studies of α-lactalbumin (Baum et al., 1989), tryptophan synthetase β_2 (Goldberg et al., 1990), cytochrome *c* (Jeng et al., 1990), apocytochrome b_{562} (Feng et al., 1991), T4 lysozyme (Lu & Dahlquist, 1992), and heat shock protein 73 (hsp73) (Palleros et al., 1992). It has also been found that disruption of disulfide bonds in α-lactalbumin (Ewbank & Creighton, 1991) and lysozyme (Radford et al., 1991) contributes to destabilization of the native state and a shift to the molten globule state(s).

Platelet factor 4 (PF4),[1] known for its heparin-binding activity (Loscalzo et al., 1985), is a platelet-specific protein of 70 amino acid residues (7800 Da) (Deuel et al., 1977). In aqueous solution, native platelet factor 4, whose structure is stabilized by the presence of two disulfide bonds (Holt et al., 1986), folds with a C-terminal α-helix stacked onto an extensive antiparallel β-sheet structural scaffold. This β-sheet domain

† This work was supported by a grant from the National Heart, Lung, and Blood Institute (HL-43194) and benefitted from NMR facilities made available through Grant RR-04040 from the National Institutes of Health.

* Address correspondence to this author.

[1] Abbreviations: PF4, platelet factor 4; NMR, nuclear magnetic resonance spectroscopy; 2D-NMR, two-dimensional NMR spectroscopy; NOESY, 2D-NMR nuclear Overhauser effect spectroscopy; NOE, nuclear Overhauser effect; rf, radio frequency; FID, free induction decay; CD, circular dichroism; HPLC, high-performance liquid chromatography; M, monomer; D, dimer; T, tetramer.

0006-2960/92/0431-12255$03.00/0

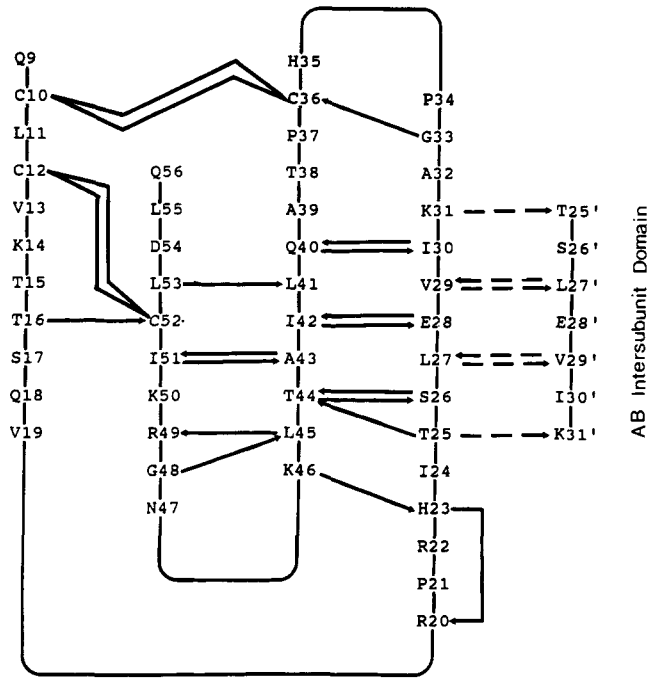

FIGURE 1: Schematic of PF4 antiparallel β-sheet domain. A schematic representation of the PF4 backbone folding is shown. N- and C-terminal conformations are omitted for clarity in showing the intrasubunit antiparallel β-sheet domain as discussed in the text. The AC dimer interface would lie below the plane of the figure. Part of the AB dimer interface showing the intersubunit antiparallel β-sheet region is given on the right of the figure. Arrows indicate H-bonds, and the double lines connecting C10 and C36 and C12 and C52 indicate disulfide linkages.

is schematized in Figure 1 for one subunit (N- and C-termini omitted). X-ray structure analysis of bovine PF4 tetramers (St. Charles et al., 1989) shows that the crystal arrangement of the four monomer subunits (identified as A, B, C, and D) is such that two types of dimers are formed, i.e., AB(CD) type and AC(BD) type. The AB dimer antiparallel β-sheet interface is partially represented in Figure 1. The AC dimer interface (not shown) would lie below the plane of the β-sheet. Two Glu–Lys salt bridges (E28/K50) and hydrophobic side-chain interactions stabilize AC-type dimers, while antiparallel β-sheet hydrogen bonds and hydrophobic interactions stabilize AB-type dimer interactions (Mayo & Chen, 1989; St. Charles et al., 1989). Native human PF4 exists in a distribution of slowly-exchanging monomer–dimer–tetramer states (Mayo & Chen, 1989).

PF4 stands as an excellent model for assessing the role that disulfides play in folding of a mostly β-sheet protein at the tertiary and quaternary structural levels. In addition, since PF4 differs in structural character from the well-studied folding "workhorse" proteins α-lactalbumin, lysozyme, and cytochromes which are more α-helix class proteins, this study may provide an added dimension to the protein folding story. In the present study, PF4 disulfide constraints were broken by chemical reduction to yield "reduced PF4" which has been analyzed by ^{1}H-NMR (600 MHz) and circular dichroism. Comparisons are made with native PF4.

MATERIALS AND METHODS

Isolation of Human PF4. For PF4, outdated human platelets were obtained from the Red Cross and centrifuged at 10000*g* for 1 h to obtain platelet-poor plasma. This preparation was applied to a heparin–agarose (Sigma) column (bed volume 50 mL); the column was washed with 0.2 M, 0.5 M, 1 M, and 1.5 M NaCl. The fraction eluting at 1.5 M NaCl which yielded most of the PF4 (Rucinski et al., 1979) was then desalted by dialysis (0.2% trifluoroacetic acid). The resulting solution was concentrated by lyophilization and further purified by HPLC as discussed in Mayo and Chen (1989). From about 50 units of outdated platelets, 20 mg of PF4 generally resulted.

Isolation of Recombinant PF4. A synthetic gene for human PF4 was synthesized and expressed as a fusion protein in *Escherichia coli*. The PF4 peptide was cleaved from the fusion protein by cyanogen bromide treatment and purified essentially as described by Myers et al. (1991) with a Vydac C-4 reverse-phase HPLC column being added as a final purification step. PF4 was eluted from the C-4 column using a water/acetonitrile gradient containing 0.1% TFA. Material eluting at approximately 40% acetonitrile was lyophilized and used in experiments. The final product was indistinguishable from human platelet derived PF4 by several criteria including heparin–agarose chromatography, isoelectric focusing, C-4 reverse-phase HPLC, gel filtration, and electrospray-mass spectroscopy analysis (Scan Inc., West Chester, PA). Human and recombinant preparations were therefore deemed to be equivalent and are referred to in the text collectively as native PF4. Recombinant protein was used exclusively for the preparation of reduced PF4.

Reduction of Native PF4. Reduced PF4 was prepared by suspending 10 mg of native PF4 in 10 mL of 6 M guanidine, 1 mM DTT, 50 mM Tris, pH 8.0. The reaction was incubated at 37 °C for 1 h. Reduced PF4 for experiments was purified by C-4 reverse-phase HPLC as described above, lyophilized, and stored under nitrogen until use. Free sulfhydryls were quantified in the final product using 7-fluoro-4-sulfamoyl-2,1,3-benzoximidazole (Toyo'oka & Imai, 1984). Reduced PF4 revealed 3.6 mol of SH/mol of protein, indicative of complete disulfide bond reduction. Analytical C-4 HPLC analysis of reduced PF4 showed production of a single product which was completely resolved from starting material. Lyophilized samples were solubilized immediately prior to the start of experiments.

Due to the potential of reduced PF4 to participate in disulfide bond formation, homogeneity was checked by HPLC analysis before and after experiments. Following a series of NMR titrations, for example, a sample of PF4 from the NMR tube was assayed by HPLC where the distribution of reduced and oxidized products can be quantified due to their different retention times in the acetonitrile gradient. In all cases, less than 5% of the material was converted back to native PF4 or other disulfide-containing intermediates that could be resolved by the HPLC column. These various other disulfides are as yet unidentified, but they probably arise from either mismatched intra- or interchain disulfide linkages.

Protein Concentration. Protein concentration was determined by the method of Lowry et al. (1951), and results were calculated from a standard dilution curve of human serum albumin. An alternative method used to determine PF4 concentration was that of Waddell (1956).

Glutaraldehyde Cross-Linking. Chemical cross-linking of PF4 oligomers was performed essentially as described by Jaenicke and Rudolph (1986). Glutaraldehyde (25%; Polysciences, Inc.) was added to 100-μL samples of either native or reduced PF4 in 0.5 M NaCl, 50 mM sodium phosphate buffer, pH 7.6. Protein concentration was held constant at 0.5 mg/mL with the final glutaraldehyde concentrations

varying from 0.1% to 1.0%. Cross-linking was allowed to proceed at room temperature for 2 min. Reactions were then terminated by addition of 1.0 mg of solid $NaBH_4$. Samples were incubated at room temperature for an additional 20 min and lyophilized. The residues were suspended in 200 μL of SDS sample buffer, and aliquots were loaded onto a 15% SDS–polyacrylamide gel.

Nuclear Magnetic Resonance (NMR) Spectroscopy. Samples for ^{1}H-NMR measurements had been lyophilized and redissolved in ^2H_2O immediately before the experiment. The final protein concentration ranged from 2 mg/mL to 16 mg/mL as indicated in the text. The p^{2}H was adjusted by adding microliter increments of NaO^{2}H or ^{2}HCl to a 0.6-mL sample. All measurements were done at the p^{2}H value indicated in the text read directly from the pH meter and not adjusted for isotope effects.

^{1}H-NMR spectra were recorded in the Fourier mode on a Bruker AMX-600 spectrometer (600 MHz for protons). The solvent deuterium signal was used as a field-frequency lock. All chemical shifts are quoted in parts per million (ppm) downfield from sodium 4,4-dimethyl-4-silapentane-1-sulfonate (DSS).

Two-dimensional NOESY (Jeener et al., 1979) NMR spectra (mixing time of 0.2 s) were accumulated in ^2H_2O as 512 time incremented, 1024 point spectra in the phase-sensitive mode (States et al., 1982). Data processing was done on the Bruker X32 computer with Bruker-supplied software. FIDs were first multiplied by a Lorentzian/Gaussian transformation or shifted sine-bell function, and data sets were zero-filled to 1024 in the evolution dimension.

Gaussian/Lorentzian Line-Shape Analysis. Resonance area integrals were derived by Gaussian/Lorentzian line fitting of NMR spectra. These procedures were done on a Sun Sparc workstation with standard Gaussian/Lorentzian functions. A part of the NMR spectrum containing the frequency region of interest was transferred to the workstation. Monomer and dimer chemical shifts, line widths, and resonance intensities were initially estimated from spectral tracings and input into the fitting program. A baseline was established by comparing fits with the noise level where no resonances were found on both sides of the aromatic resonance region. Baselines were generally flat. Derived areas from these fits varied from sample to sample by no more than about 5%.

Amide H/D Exchange. The exchange rates of the amide protons for deuterons of the deuterium oxide solvent were determined by measuring the time-dependent decrease of ^{1}H NMR line intensities as protons were replaced by deuterons. Resonance intensities were measured and calibrated relative to those of Y60 ring proton resonances. The accuracy of these measurements is estimated to be about ±20%. The experimental decay of the resonances was plotted as pseudo-first-order kinetics. In cases of multiphasic decay curves, estimates of exchange kinetics were made by measuring the initial and final slopes.

Circular Dichroism. Circular dichroic (CD) spectra were measured on a Jobin-Yvon CD-6 automatic recording spectropolarimeter coupled with a data processor. Curves were recorded digitally and fed through the data processor for signal averaging and baseline subtraction. Spectra were recorded at 20 °C in 10 mM phosphate buffer, pH 3 and 6, over 190–310 nm using a 2-mm-path-length quartz cuvette. PF4 concentration was 2–4 μM. The scan speed was 5.0 nm/min. Spectra were signal-averaged four times, and an equally signal-averaged solvent baseline was subtracted. CD spectra were analyzed by the Provencher program for protein secondary structure prediction (Provencher & Glöckner, 1981; Provencher, 1982).

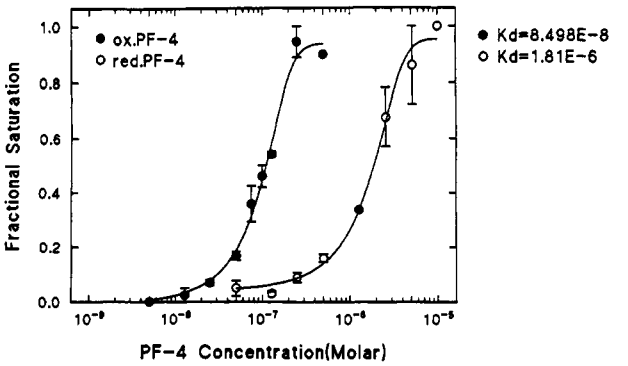

FIGURE 2: Heparin binding to reduced and native PF4. Heparin–PF4 complex formation was examined over a range of PF4 concentrations in the presence of a fixed concentration of tritiated-heparin as explained in the Materials and Methods section. This was done for both native and reduced species of PF4 as labeled in the figure. K_d calculations were made at half-saturation with the aid of the P-FIT computer program. Experimental points are the average of three determinations. Error bars indicate standard deviation from the mean.

Heparin Binding to PF4. Heparin–PF4 complex formation was examined over a wide range of PF4 concentrations in the presence of a fixed concentration of [^{3}H(G)]heparin (NEN; 0.29 mCi/mg). Reactions were carried out in 0.5 mL of 10 mM Tris-HCl, pH 8.0, containing 40 μg/mL bovine serum albumin. After a 45-min incubation at room temperature, samples were passed through a 0.1-μm nitrocellulose filter which retained [^{3}H]heparin–PF4 complexes but not free [^{3}H]-heparin. Filters were dried and then solubilized with scintillation fluid and counted. K_d calculations were made at half-saturation with the aid of the P-FIT computer program.

RESULTS

Heparin Binding to PF4. Chemical reduction of the two disulfide bonds in PF4 causes substantial changes in PF4 structure as evidenced by decreased affinity for heparin. These results are presented in Figure 2 as a comparison of heparin–PF4 complex formation over a range of protein concentrations. Association equilibrium binding constants to heparin, K_{hep}, taken at half-saturation are 11.8×10^6 M^{-1} and 0.6×10^6 M^{-1} for native and reduced species, respectively. This represents a 20-fold decrease in apparent affinities. No significant changes in the binding curve for reduced PF4 were observed even when the protein was used in experiments several hours after solubilization. This suggests that the majority of the material has not refolded back to the native conformation during this time frame. This was confirmed by HPLC analysis as described in Materials and Methods.

Dimerization of Reduced PF4. Gel filtration profiles of reduced PF4 and native PF4 show significant differences suggesting sulfhydryl-dependent changes in aggregation state (Figure 3). Apparent molecular weights for native and reduced PF4 are 28 000 and 21 700, respectively. On the basis of a monomer molecular weight of 7800, these sizes suggest tetramer and trimer aggregation states. This interpretation assumes both types of monomers exhibit ideal column behavior. To clarify this point, both proteins were chemically cross-linked with glutaraldehyde and analyzed by SDS gel electrophoresis under reducing conditions where both monomers would presumably have an equal contribution to the observed molecular weight of the aggregate forms. Figure 4 shows that under conditions where native PF4 is quantitatively cross-

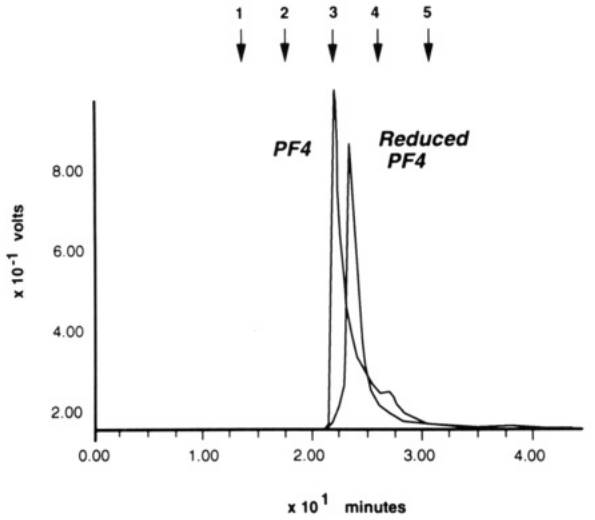

FIGURE 3: Gel filtration of normal and reduced PF4. Fifty-microgram samples of reduced PF4 and native PF4 were chromatographed on a Superose 12 FPLC column equilibrated in 0.5 M NaCl, 50 mM $NaPO_4$ buffer, pH 7.6. Elution positions of molecular weight standards are indicated: BSA, 66 000; carbonic anhydrase, 29 000; cytochrome *c*, 12 000; aprotinin, 6500. Apparent molecular weights of native and reduced PF4 are 28 400 and 21 700, respectively.

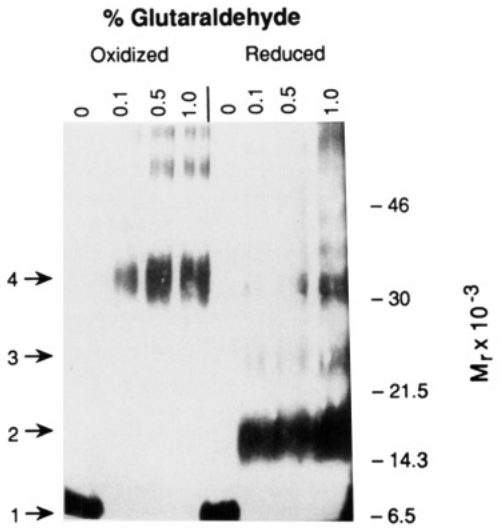

FIGURE 4: Chemical cross-linking of PF4 multimers. SDS denaturing gels are shown for native and reduced PF4 which had been reacted in the presence and absence of glutaraldehyde cross-linker. Reactions were run as described in the Materials and Methods section; 20-μL samples were loaded on a 15% SDS–polyacrylamide gel. Following electrophoresis, the proteins were visualized with silver stain. Positions of molecular weight standards are indicated along with the predicted elution for monomer, dimer, trimer, and tetramer PF4.

linked to a tetramer, reduced PF4 shows predominantly dimer as its highest aggregation state.

Like native human PF4 (Mayo & Chen, 1989) and low-affinity PF4 (Mayo, 1991), reduced PF4 demonstrates pH-dependent proton NMR spectral intensity changes. Figure 5 shows the aromatic and partial αH NMR spectral region of reduced PF4. The aromatic resonance region is simple since it contains only ring proton resonances from Y60, H23, and H35. As the pH is increased from 2.8, the relatively narrow Y60 2,6 and 3,5 doublet resonances (Mayo & Chen, 1989) are slightly broadened and decrease in intensity while a second resonance set for Y60 appears and dominates the Y60 resonance populations by pH 5. Y60 2,6 and 3,5 ring proton resonances have been grouped by using 2D-NMR COSY and NOESY spectra (data not shown). At pH values

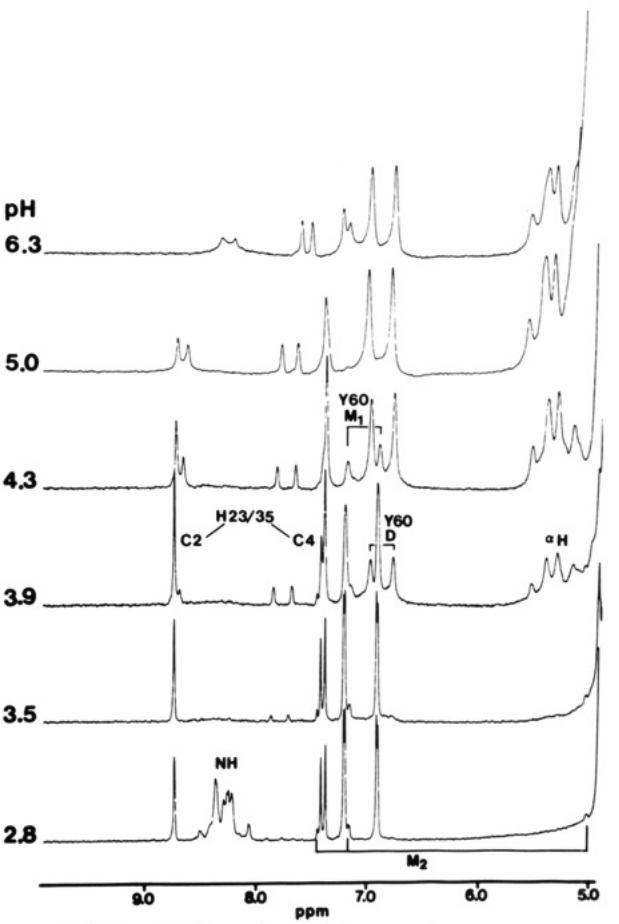

FIGURE 5: Effect of pH on reduced PF4 aromatic proton resonances. A series of proton NMR spectra (600 MHz) taken in ^2H_2O are shown for the reduced PF4 aromatic resonance region as a function of solution pH indicated in the figure next to each spectrum. The reduced PF4 concentration was 6 mg/mL. The temperature was 303 K. The resonance label prefixes M and D stand for monomer and dimer states, respectively.

where both resonance sets can be observed, i.e., pH 4.3, concentration-dependent resonance integral changes (data not shown) give Hill plot slopes of 1.8–2.1 indicative of dimer formation as observed above in cross-linking experiments. Other non-tyrosine resonances in Figure 5 must belong to His 23 and His 35 C2 and C4 ring proton resonances and various αH resonances. Therefore, as with native PF4 (Mayo & Chen, 1989), Y60, H23, and H35 ring proton resonances have been assigned to monomer and dimer states as shown in Figure 5. The apparent increase in reduced PF4 monomer Y60 resonance line widths mentioned above is probably the result of chemical exchange broadening as monomer and dimer species associate and dissociate. This has been previously observed with native PF4 (Chen & Mayo, 1991).

No tetramer state Y60 resonances were observed at any pH value investigated. It could be that tetramer state resonances represent a small population of the total protein which either overlaps other resonances or falls within spectral noise. If tetramer Y60 resonances were overlapping with others, their intensity could be no more than the error in fitting resonance integrals, i.e., less than about 5%. This is consistent with chemical cross-linking data discussed earlier.

At lower pH values, a set of minor resonances is apparent. These similarly intense resonances are seen at the upfield side of the Y60 2,6 resonance, at the downfield side of the histidine C4 resonances, and in the αH region. Since their relative intensities are PF4 concentration independent, they presum-

ably represent a subpopulation (about 5%) of monomer PF4. These major and minor monomer states are called M_1 and M_2, respectively.

At pH 2.8 (Figure 5), some relatively long-lived NH resonances associated with the reduced PF4 monomer state are present between 8 and 8.5 ppm. They are absent at higher pH values in this figure since they were allowed to exchange prior to continuation of the pH titration. These relatively long-lived NHs will be discussed later.

Figure 5 also suggests that H23 and H35 pK_as for reduced PF4 dimers both fall around pH 6. Since only a partial titration curve resulted due to limited solubility of reduced PF4 at higher pH values and low ionic strength, these pK_as were estimated by assuming a 1 ppm C2-proton chemical shift difference between acidic and basic forms of histidine. Previous tentative assignments for the two histidines, His I and II, (Mayo & Chen, 1989) have now been assigned by sequential resonance assignment methods as H23 and H35, respectively (unpublished results). For native PF4 (Mayo & Chen, 1989), the H35 pK_a in all aggregate states was also around pH 6, while the pK_a for H23 was below pH 5. This suggests that H23 may be somehow involved in, or at least responsive to, the association process. Alternatively, it could mean that conformational perturbations induced by disulfide reduction cause a H23 pK_a shift. In addition, the appearance of two resonances at 7.75 and 7.9 ppm parallel the growth of reduced dimer species (Figure 5). These seem to be associated with histidine C2 resonance populations due to similar pH-induced chemical shift behavior and to equal intensity (in the absence of monomer species) with more downfield histidine resonances. In fact, a total histidine resonance intensity of 2 protons (relative to that of Y60 resonances) is only achieved when these resonances are included. This effect is reversible on lowering the pH. The origin of these resonances, however, is unclear, but they may represent slowly exchanging multiple histidine conformation states. A similar effect was previously observed for native PF4 (Mayo & Chen, 1989).

Association Equilibrium Constants. As discussed by Mayo and Chen (1989), apparent equilibrium constants for dimer association can be derived from these steady-state M and D populations from consideration of the general equilibrium expression

$$K_D = [D]/[M]^2 \quad (1)$$

Knowing the mole fraction of M and D derived from resonance integrals and the total protein concentration per mole of Y60, i.e., per mole of subunit, allows one to calculate K_D. The monomer population derived from these NMR experiments is actually the M_1 monomer concentration of folded (M_f) and unfolded (M_u) states. Normally, it is appropriately assumed that $M_f \gg M_u$. For native PF4 this assumption is justified since monomers give NMR spectra characteristic of a folded protein (Mayo & Chen, 1989). For reduced PF4, however, this assumption cannot strictly be adhered to as will be discussed later; therefore, the distinction between apparent (i.e., $[D]/[M_f + M_u]^2$) and intrinsic (i.e., $[D]/[M_f]^2$) K_D values must be emphasized.

The logarithm of apparent K_D values (filled-in squares) is plotted in Figure 6 as a function of solution pH from pH 2.3 to 5.8. As the pH is raised, K_D values increase monotonically and appear to plateau off at about pH 6. For comparison, K_D values for native PF4 (open squares) (Mayo & Chen, 1989) are also shown. The reduced PF4 K_D–pH dependence profile, while shifted slightly to lower values, parallels that observed for native PF4 dimers. The pH dependence of protein

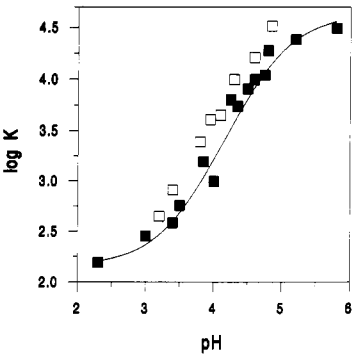

FIGURE 6: Effect of pH on equilibrium constants for reduced and native PF4. Plots are shown for reduced PF4 association equilibrium constants as log K_D versus pH (solid squares). Values for K_D were derived as discussed in the text. For comparison, equilibrium constants for native PF4 as estimated by Mayo and Chen (1989) are shown with open squares. As described in the text, the line through log K_D values represents the best fit of the data to eq 2.

association could be the result of several factors related to the nature of subunit interactions. Two types of charge interactions could cause association to decrease with decreasing pH: (1) elimination of an attractive cationic–anionic interaction by protonation of the anionic group; or (2) increasing unfavorable long-range electrostatic repulsion between two macroions with a net positive charge. To a first approximation, the Wyman (1964) ligand activity relationships help explain the pH dependence on association in terms of interactions between ionizable groups fixed in space. This type of analysis was used for the study of α-chymotrypsin dimerization (Aune et al., 1971; Aune & Timasheff, 1971) and PF4 dimerization and tetramerization (Mayo & Chen, 1989). Since the slope of log K_D vs pH in Figure 6 lies between 3 and 4, the simplest explanation is to assume that four groups are involved in the interaction. In other words, these interactions probably involve two different side chains on each subunit.

The pH dependence of the association equilibrium constant is given by (Wyman, 1964)

$$\ln K = \ln K(\mathrm{pH} = \infty) + 2 \ln \frac{(1 + a_H/K_{1,D})(1 + a_H/K_{2,D})}{(1 + a_H/K_{1,M})(1 + a_H/K_{2,M})} \quad (2)$$

where a_H is essentially given by the hydrogen ion concentration and K_1 and K_2 are the ionization constants for the interacting groups in M and D states, respectively. The data of Figure 6 were iteratively curve fitted to this expression using three variables at a time. A satisfactory fit was obtained as shown by the solid line in Figure 6 with values of p$K_{1,M}$ = 4.6 and p$K_{2,M}$ = 8.8; on dimerization the values changed to p$K_{1,D}$ = 3.4 and p$K_{2,D}$ = 10.1. These pK_a values vary significantly from those given by Mayo and Chen (1989); this is probably due to a more complete dimer/monomer K_D–pH dependence and structural differences with the native species. The pK_a values of these interacting groups are, nevertheless, most readily identified with Glu/Asp and Lys/Arg side chain ionizations as also reported for native PF4 (Mayo & Chen, 1989). The X-ray structure of bovine PF4 gives only one clear case of such intersubunit electrostatic interactions between E28 and K50. This key salt-bridge significantly contributes to the stabilization of the PF4 AC dimer. No such interactions are evident with AB-type dimers. In fact, E28–E28 electrostatic repulsion probably contributes to destabilization of AB-type dimer interactions (Mayo & Chen,

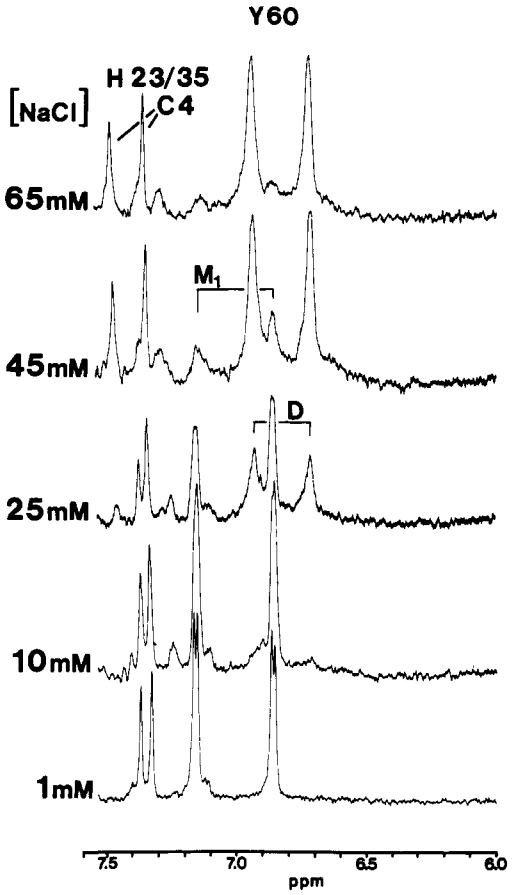

FIGURE 7: Effect of ionic strength. A series of NMR spectra (600 MHz) for the aromatic proton resonance region of reduced PF4 is shown as a function of NaCl concentration as indicated in the figure. The protein concentration was 3 mg/mL at 303 K and pH 3.1 in ^2H_2O.

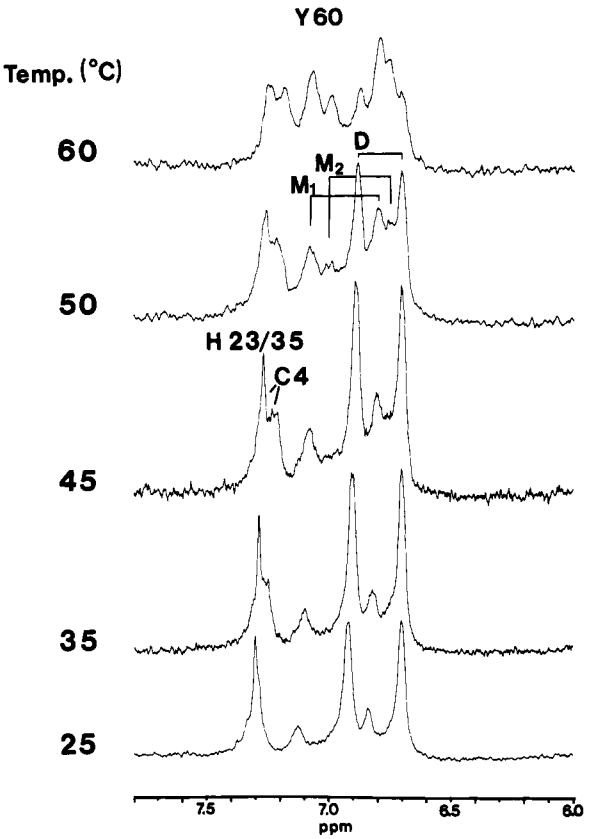

FIGURE 8: NMR spectra temperature dependence for reduced PF4. At pH 4 where all states are clearly present, the temperature dependence of ^{1}H-NMR (600 MHz) spectra for reduced PF4 was monitored. NMR spectra were accumulated as discussed in the Figure 5 legend and in the text.

1989). As far as this present study is concerned, it seems that the general nature of monomer–monomer interactions is conserved in native and reduced PF4 species.

Effect of NaCl on Dimerization. Figure 7 gives a series of NMR spectra at pH 3.1 and at a fixed reduced PF4 concentration (3 mg/mL) as a function of NaCl concentration. At low ionic strength, only reduced PF4 monomer is observed. At 25 mM NaCl, the monomer–dimer equilibrium is shifted in favor of the dimer state. Monomer resonance broadening is likely due to chemical exchange between monomer and dimer species (Chen & Mayo, 1991). On addition of 65 mM salt and above, the equilibrium is shifted almost totally to the dimer state. Similar results were also obtained at pH 4.9 (data not shown), i.e., increasing ionic strength shifts the monomer–dimer equilibrium to the dimer state. The overall effect, however, is greater at lower pH. Once again, this parallels what has been observed with native PF4 (Mayo & Chen, 1989), and as with native PF4, this salt effect suggests that forces other than electrostatic ones, i.e., hydrophobic, are also integrally involved in the monomer–monomer subunit interface and dimer stability. This is consistent with what is known regarding PF4 quaternary structure (St. Charles et al., 1989).

Effect of Temperature. Typical temperature effects on monomer and dimer state distributions are shown in NMR spectra in Figure 8. From 20 °C to 40 °C, reduced monomer and dimer populations remain fairly unchanged like those for native PF4 (Chen & Mayo, 1991). Within this narrow temperature range, a very small change in overall average enthalpy seems to figure into the subunit association process. Since the free energy of association, ΔG, is negative, the net entropic contribution must be positive. Ross and Subramanian (1981) have indicated that such trends in association thermodynamic parameters relate to electrostatic charge neutralization in a low dielectric constant medium (like within a protein core) and/or hydrophobic interactions. Both electrostatic and hydrophobic interactions contribute to the stabilization of AC-type dimers. This again supports the proposal that monomer–monomer interactions are similar between native and reduced species.

Above 40 °C, the reduced PF4 temperature dependence shows pronounced differences with respect to native PF4 (Chen & Mayo, 1991). For reduced PF4, subunit exchange remains slow on the 600-MHz ^{1}H-NMR time scale even up to 60 °C, while for native PF4, the 500 MHz (Chen & Mayo, 1991) or 600 MHz (unpublished results) fast chemical exchange regime is reached by 60 °C. Assuming a diffusion-limited forward rate, this indicates that the reduced PF4 dimer state lifetime is somewhat longer than its native counterpart and suggests that although dimer subunit interactions are similar as mentioned above, differences do exist. Furthermore, with increasing temperature, the reduced PF4 dimer population is gradually decreased as M_1 and M_2 monomer populations are increased. Figure 9 plots these changes as ln K_D and fraction M_1 and M_2 versus the inverse temperature in Kelvin, K^{-1}. Assuming a linear slope for ln K_D vs $1/T$, the van't Hoff plot yields an apparent ΔH_D of association of –23 kcal/mol. At 60 °C, therefore, ΔG_D (apparent) = –4.5 kcal/mol and ΔS_D (apparent) = –55 cal/mol·K. This might suggest increased solvation of the protein "interior" brought about by the unfolding process at higher temperatures. Notice also the parallel growth of M_1 and M_2 with the ratio of M_2/M_1

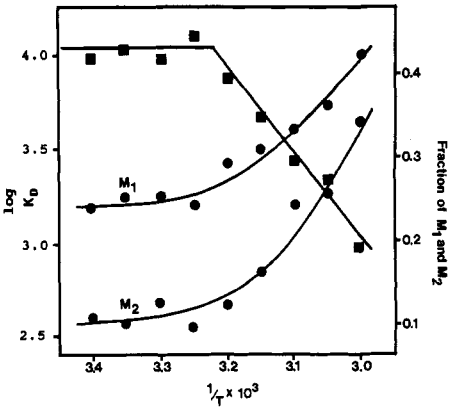

FIGURE 9: Plots of ln K_D and fraction monomer versus K^{-1}. From NMR data like those shown in Figure 8, the natural logarithm of apparent K_D is plotted versus the inverse temperature in Kelvin. The monomer population is taken as $M_1 + M_2$ as discussed in the text. M_1 and M_2 fractional populations are also plotted. Lines drawn through points are for visual aid only.

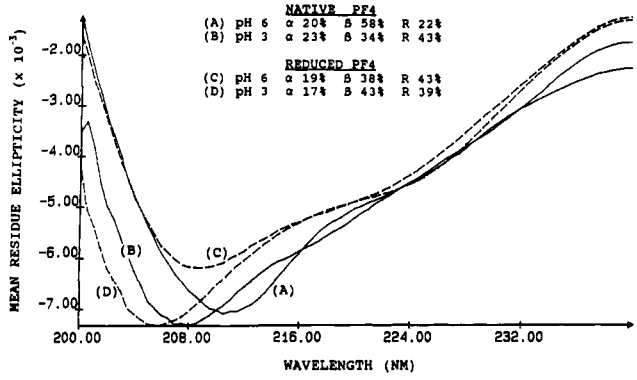

FIGURE 10: Far-ultraviolet CD spectra of PF4. Circular dichroic spectra for PF4 in reduced and native states are shown as mean residue ellipticity versus wavelength (in nanometers). PF4 concentration is 2 μM in 10 mM phosphate buffer. The pH was adjusted to pH 3 and 6 as indicated in the figure. The temperature was controlled at 20 °C. Other experimental variables are given in the Materials and Methods section.

increasing only slightly with increasing temperature. This suggests the presence of mainly entropic differences between these two monomer states. For native PF4, temperature-induced aggregate state population changes above 40 °C could not be followed due to the onset of intermediate and fast chemical exchange (Chen & Mayo, 1991).

Structural Differences between Reduced and Native PF4. From data presented above, it is apparent that monomer subunit structure within the reduced PF4 dimer state is very similar to that in native PF4. This is supported by CD data in Figure 10 which compare reduced and native PF4. At pH 6, where native PF4 is in the tetramer state (Mayo & Chen, 1989) and reduced PF4 is in the dimer state, deconvolution of CD traces gives essentially the same helix composition and about 20% less β-sheet structure for the reduced species (38% compared to 58%). Although the origin of this average β-sheet difference is unknown, this observation is consistent with disulfide reduction-induced structural perturbations which are most evident in the apparent absence of reduced PF4 tetramer species.

Figure 11 shows several ^{1}H-NMR spectra for reduced and native PF4 monomer species. For reference, native tetramer PF4 (bottom trace) shows a number of well-dispersed, long-lived backbone amide proton resonances and several downfield-shifted NH and αH resonances. NMR conformational analysis (results to be published elsewhere) indicates that these

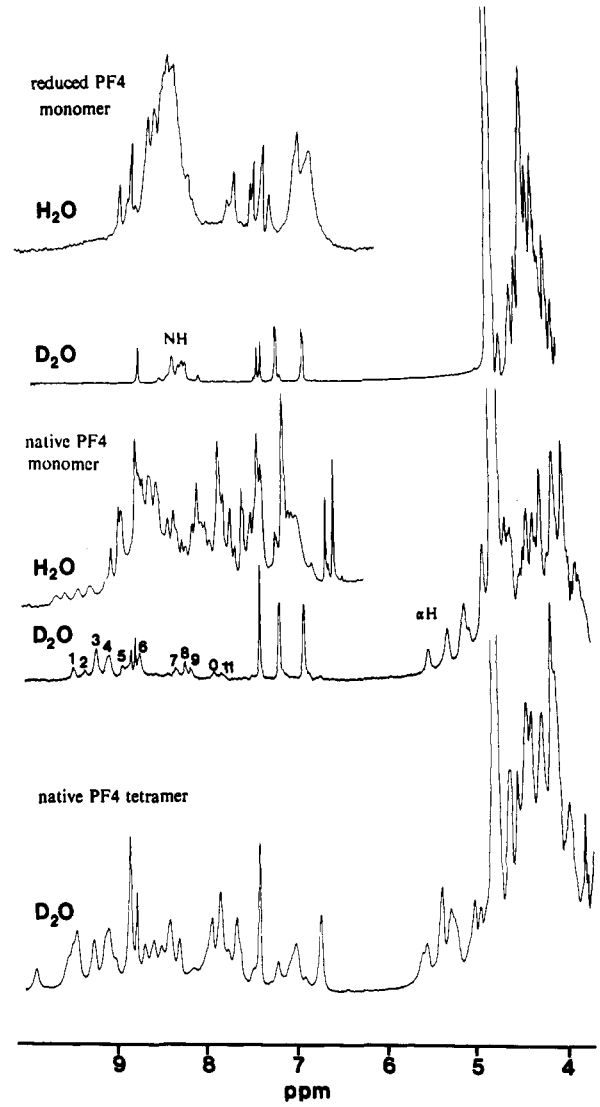

FIGURE 11: NMR spectra of reduced and native PF4. The 600 MHz proton NMR spectra of native tetramer and monomer PF4 and reduced monomer PF4 are shown as labeled. Lyophilized protein samples were dissolved in ^2H_2O at pH 3, 303 K, containing PF4 concentrations ranging from 2–4 mg/mL for monomer species to 16 mg/mL for the tetramer. Inserts showing the downfield NH spectral region for PF4 dissolved in 90% ^1H_2O/10% ^2H_2O are also included. No buffer or salt was added to these solutions.

downfield-shifted NH and αH resonances result from antiparallel β-sheet structure. A 2D-NMR NOESY contour plot of the αH region (Figure 12) shows some αH–αH connectivities characteristic of this structural motif. Native PF4 monomers apparently have these same structural features as evidenced by a similar NOESY αH–αH region (Figure 12) and similarly well-dispersed, long-lived NH resonances (Figure 11). For reduced PF4 dimers, comparable downfield-shifted αH resonances (Figure 5) and 2D-NMR NOESY αH–αH region contour plots (data not shown) also indicate preservation of this antiparallel β-sheet folding motif.

Reduced PF4 monomers, on the other hand, lack these spectral features. Figure 11 indicates that normally downfield-shifted αH and NH resonances have been apparently shifted upfield. Even NMR spectra recorded in 90% ^1H_2O/10% ^2H_2O (Figure 11 inserts) show the absence of structurally suggestive, downfield-shifted NH resonances. Combined with the presence of relatively narrower resonance line widths, this suggests a more unfolded or less structured conformation for the reduced PF4 monomer state. Since the degree of unfolding cannot be

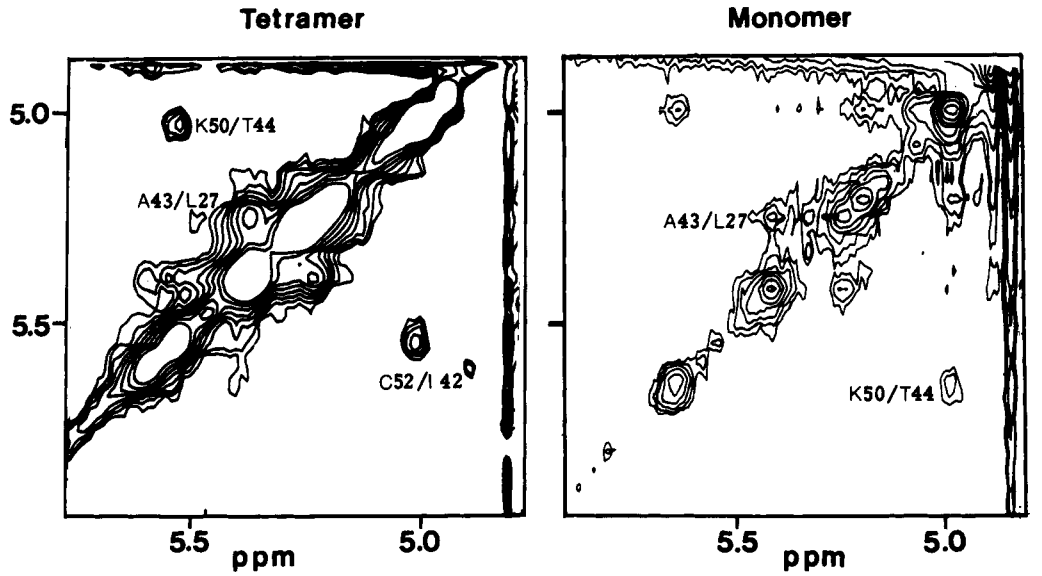

FIGURE 12: 2D-NMR contour plots of αH–αH resonance region. The αH–αH resonance region of NOESY contour plots of native PF4 monomer and tetramer states are shown. The mixing time was 0.2 s. The solution pH was 3. The temperature was 303 K. Other experimental details are given in the Materials and Methods section.

established from these NMR data, far-ultraviolet CD spectra of reduced and native PF4 monomers (pH 3) are shown in Figure 10 (traces B and D). In both cases, CD spectra are similar showing negative ellipticities and differing appreciably from CD spectra of proteins known to assume random-coil conformations in solution (Brahms & Brahms, 1980; Johnson, 1988, and references cited therein) as NMR data suggest. Of particular note, the CD trace for reduced PF4 monomer gives evidence of significant secondary structure. Gaussian deconvolution of these CD spectra (Provencher & Glöckner, 1981; Provencher, 1982) yields distributions of percent α-helix, β-structure, and random coil (or better remainder (R)) as tabulated in Figure 10. The only major change in secondary structural composition with respect to native PF4 tetrameric state (Figure 12, trace A) lies in decreased β-structure which drops from 58% to 34% and 43%, respectively. A similar drop in β-sheet structural composition was noted above for the reduced PF4 dimer state. Helix content which originates mostly from the C-terminal domain is preserved regardless of the presence/absence of disulfide bonds. Due to the presence of only one tyrosine, i.e., Y60, near-UV CD region (260–310 nm) was uninformative regarding the observation of tertiary structural differences (Baum et al., 1989).

Additionally, the observation of long-lived amides (Figures 5 and 11) supports the presence of some "folded" structure in reduced PF4 monomer state. In guinea pig α-lactalbumin, Baum et al. (1989), for example, found that two segments which form α-helices in the native conformation have protected amide protons in the molten globule state. For reduced PF4, specific structural elements to which these long-lived NHs are associated are as yet unidentified. Figure 13 gives four NMR spectra exemplifying the time course for reduced PF4 monomer H/D exchange. The initial NMR spectrum (bottom) indicates that about 40 NH backbone protons (estimated from relative integrated area) are still present within 20 min after reduced PF4 is dissolved in deuterium oxide at pH 3.2 and 25 °C. Most of these NHs (about 70%) exchange rapidly within 40 min and may be attributable to H/D exchange within solvent-exposed, random-coil structure, i.e., equivalent to intrinsic exchange defined by Englander and Poulsen (1969). The intrinsic H/D exchange rate under these experimental conditions is estimated to be 20×10^{-4} s^{-1} by the Englander

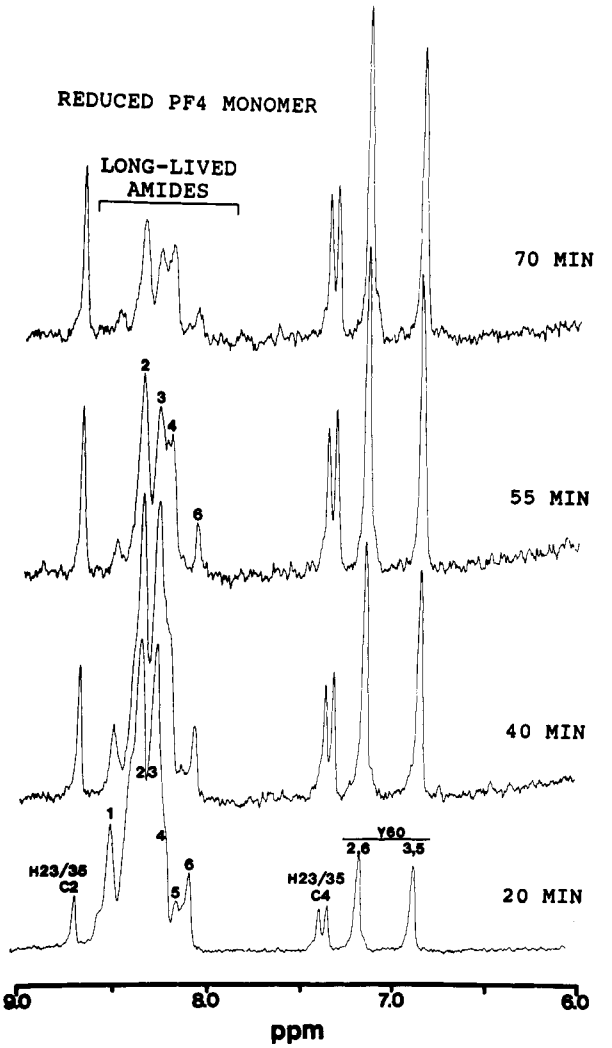

FIGURE 13: Amide exchange for reduced PF4. Four NMR spectra exemplifying NH/ND exchange for reduced PF4 monomer state are given. The first spectrum was accumulated within 20 min of dissolving 4 mg/mL of reduced PF4 in deuterium oxide. Additional NMR spectra (256 transients each) were accumulated every 7 min. The solution pH (measured after the experiment) was 3, and the temperature was controlled at 25 °C.

Table I: Amide Exchange Rates for Reduced and Native PF4 Monomers at pH 3 and 25 °C

reduced PF4 monomers		native PF4 monomers	
res no.[a]	apparent exchange rate ($\times 10^5$ s^{-1})	res no.[a]	apparent exchange rate ($\times 10^5$ s^{-1})
1	260 (3)[b] and 16 (1)[b]	1	8
2	180 (12)[b] and 60 (4)[b]	2	25
3	180 (11)[b] and 50 (3)[b]	3[c]	≈5 and 15
4	35 (2)[b]	4[c]	≈5 and 20
5	40 (1)[b]	5	10
6	153 (1)[b] and 28 (1)[b]	6[c]	≈10 and 40
		7	35
		8	17
		9	23
		10	28
		11	60

[a] Arbitrary resonance numbers are given from downfield to upfield for resonances labeled in Figure 12. [b] An estimate of the number of exchanging amides in a given resonance envelope is given in parentheses. [c] These resonances for native PF4 show biphasic kinetic exchange curves; apparent exchange rate constants have been estimated from initial and final slopes of these curves. All other resonances for native PF4 monomer are apparently single resonances.

and Poulsen (1969) empirical equation for solvent-accessible amide protons in model peptides. Decay curves for some are multiphasic (data not shown), and only estimates of exchange rate constants can be obtained from extreme slopes of these curves. These values are given in Table I for NH resonances labeled in Figure 13. Some 12 backbone amides exchange 3–12 times slower than this rate and can be considered relatively long-lived. For comparison, exchange rates for native PF4 monomers have also been measured at pH 3 and 25 °C and are listed in Table I for NH resonances labeled in Figure 11. Many of these long-lived NHs for native PF4 monomers are associated with protons in antiparallel β-sheet structure (unpublished results; see Figures 11 and 12). Interestingly, these native PF4 monomer exchange rates, while normally slower, are similar to those found for the 12 or so long-lived NHs in reduced PF4 monomers (Table I), suggesting the presence of some structure folding in reduced PF4 monomers. It might also be added that exchange rates for native PF4 monomer are by themselves considerably faster than those observed for what one may consider "rigid" proteins of comparable molecular weight where NH lifetimes can be measured in days. Qualitatively, this seems to suggest that even native PF4 monomers are relatively structurally flexible.

Taken together, CD and NMR data indicate that reduced PF4 monomers possess considerable secondary structure but lack tertiary structural detail as observed for the native monomeric state. These observations are consistent with reduced PF4 monomers existing in some type of "molten globule" state. As further evidence, however, that this monomeric state is a "molten globule" intermediate and is not fully "unfolded", reduced PF4 monomers were titrated with a protein denaturant, urea. Baum et al. (1989) have characterized the molten globule (pH 2) and unfolded (urea) states of α-lactalbumin and found significant line-width and chemical shift differences between these two states. α-Lactalbumin, however, is twice the molecular weight of monomer PF4, i.e., 14 000, and contains many more internalized, aromatic residues which are more sensitive to tertiary structural interactions (Baum et al., 1989). The sparcity of such aromatic residue "folding probes" in the smaller protein PF4 (with one tyrosine and two histidines) means that such characteristic spectral changes will be less apparent.

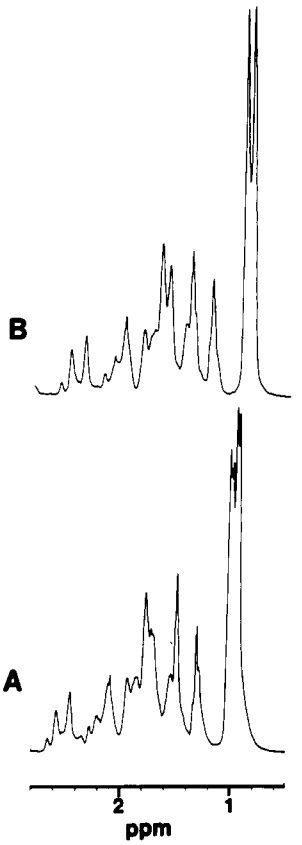

FIGURE 14: NMR spectra showing upfield aliphatic methyl region. The upfield aliphatic methyl region from NMR spectra of reduced PF4 monomer in the absence (A) and presence (B) of 9 M urea is shown. Solution conditions are as described in the Figure 11 legend.

Addition of 9 M urea to reduced PF4 monomers does induce chemical shifts in some resonances, although general spectral features are similar. Y60 resonances which already resonate within random-coil shift limits in the native species show little change in this regard. This is not too surprising since Y60 has been shown to be solvent exposed in native PF4 monomers and more internalized in the tetramer state (Mayo & Chen, 1989). Line widths of the only single resonances in the spectra, i.e., Y60, H23, and H35, also do not appear to be affected by urea denaturation. On reduction of native PF4, Y60 line-width changes of only about 1 Hz were noted (see Figure 11). Line-width changes of resonances in the upfield region are difficult to discern due to the nature of overlapping resonances, but changes, if they do occur, are apparently minimal. Significant chemical shift changes are noted, however, for specific upfield resonance envelopes (Figure 14), while others remain unperturbed. Surprisingly, significant chemical shift changes are observed within the aliphatic methyl region around 1 ppm. Here, in the presence of 9 M urea, methyl resonances are less dispersed and more in line with expected random-coil chemical shifts. Many of these methyls belong to hydrophobic residues found in the interior of folded PF4 (St. Charles et al., 1989). This is consistent with reduced PF4 monomer being identified as an intermediate folded state.

The presence of molten globule monomers prior to dimerization indicates that the reduced PF4 folding transition is thermodynamically linked with dimer formation. This is clearly observed in Figure 5 where the appearance of downfield-shifted αH resonances parallels the growth in dimer state population and indicates that antiparallel β-sheet folded structure has formed upon dimerization.

DISCUSSION

In this study, there is a clear interplay of protein folding, subunit association, and the effect of disulfide bonds on both. Reduction of disulfide bonds in PF4 shifts the native monomer conformation into an intermediate structural state(s), most closely resembling that defined as a molten globule (Ptitsyn, 1987; Kuwajima, 1989). Molten globule intermediate structures are compact and have substantial secondary conformation but few if any fixed tertiary interactions. For reduced PF4 monomers, "loosening" of the "fixed" tertiary structure is evidenced by highly upfield-shifted NH and αH resonances and narrower resonance line widths. Preservation of secondary structure is indicated by CD spectra and the presence of long-lived backbone NHs. Apparently, the cystine oxidation state plays a minor role in secondary structure formation but a major role in tertiary structure stabilization and folding.

Molten globule intermediates may be viewed either as collapsed, unfolded states (Goldberg et al., 1990; Ewbank & Creighton, 1991) or as an expanded native state which maintains its overall backbone fold (Baum et al., 1989; Hughson et al., 1990). While the present data on PF4 are compatible with either view, they do suggest that the molten globule state(s) should have some temporal native PF4 character in order to explain very similar native and reduced PF4 dimer K_D values. In this respect, whatever pre-dimer intermediate monomer states are present, they should be rapidly interconverting on a time scale which is much faster than the NMR slow exchange time scale observed for monomer–dimer equilibria (about 10 ms).

Quaternary structure formation is not often discussed in the context of protein folding, but it is in any event a further step in the folding process. Since breaking disulfide bonds destabilizes native PF4 monomeric structure, one might expect that reduced PF4 quaternary structure would likewise be affected. In this respect, reduced PF4 tetramers, if they can form, have not been observed in NMR or chemical cross-linking experiments, indicating at best a large decrease in dimer–dimer equilibrium association constants (Mayo & Chen, 1989). On the other hand, formation of a highly structured, reduced PF4 dimer state from an apparent molten globule intermediate indicates that the PF4 folding transition, in the absence of disulfides, is thermodynamically linked with dimer formation. Reduced PF4 dimers define a stable intermediate quaternary structure since native PF4 tetramers represent the final folded state. De Francesco et al. (1991) have also found that dimerization of a normally random coil, 32-residue peptide fragment from transcription protein LFB1 induces stable subunit structure.

Of the two main types of PF4 dimers that could form in solution, i.e., AB and AC, the AC-type dimer for native PF4 has been proposed as being more thermodynamically favored (Mayo & Chen, 1989; Chen & Mayo, 1991). These present results also indicate formation of the same type dimers with reduced PF4. Apparent differences between the strength of reduced and native PF4 subunit interactions suggest that cystine reduction induces some conformational differences in the dimer state. The dimer–dimer intersubunit domain, on the other hand, must be highly perturbed since reduction significantly inhibits, if not prohibits, normal native PF4 tetramer formation (see Figure 1) (Mayo & Chen, 1989; Chen & Mayo, 1991). The main difference between reduced and native PF4 quaternary structure, therefore, lies in dimer–dimer (tetramer) association.

The region which is most associated with the AB-type dimer contact domain is the β-sheet segment I24 to G33 in chain A running antiparallel to the same segment in opposing chain B. The main elements of this antiparallel β-sheet conformation (see Figure 1) must be preserved in the absence of disulfide bonds since reduced PF4 AC dimers still form. This in turn indicates that one or both of the cystine disulfide bonds influence more localized structure of some portion of that β-sheet conformation. Notice that while the C10–C36 disulfide bond anchors the N-terminus to one side of the intrasubunit, antiparallel β-sheet domain, the C12–C52 disulfide bond anchors the other side of the same domain. In at least bovine PF4, the G48–C51 (G33–C36 in human PF4) turn which leads out of the AB dimer intersubunit, antiparallel β-sheet domain, forms an atypical 14-atom turn with the CO of C51 hydrogen bonding to the NH of G48 (St. Charles et al., 1989). This unusual turn conformation could be due to conformational restrictions from the C25–C51 disulfide bond. Since it connects two β-sheet segments, one of which forms the AB dimer interface, disruption of the C12–C52 disulfide bond could induce sufficient deformation in the normally aligned intersubunit, antiparallel β-sheet segments of the AB-dimer interface to account for these observations. Kuwajima et al. (1990) have found that the superreactivity of the C6–C120 disulfide bond in α-lactalbumin results from geometric strain imposed on the disulfide bond by the native structure folding. For human tissue plasminogen activator, Opitz et al. (1987) have stated that disulfide bridges do not determine the spatial arrangement of the backbone but rather act only to stabilize the structure. Alternatively, one could ask whether the disulfide bond places a strain on the peptide backbone conformation. In human PF4, the C10–C36 disulfide bond could be inducing torsional strain on the peptide backbone which could affect antiparallel β-sheet alignment and account for differences in the strength of subunit interactions. For PF4, disulfides apparently have a dual role: stabilize monomer folds and determine/restrain local structure. The precise reason for this will have to await complete NMR structure elucidation and comparison of both proteins, which is currently underway.

ACKNOWLEDGMENT

We gratefully acknowledge the expertise of Dr. Robert C. Blanks for quality control analysis of PF4 samples.

REFERENCES

Aune, K. C., & Timasheff, S. N. (1971) *Biochemistry 10*, 1609–1617.

Aune, K. C., Goldsmith, L. C., & Timasheff, S. N. (1971) *Biochemistry 10*, 1617–1625.

Baum, J., Dobson, C. M., Evas, P. A., & Hanley, C. (1989) *Biochemistry 28*, 7–13.

Brahms, S., & Brahms, J. (1980) *J. Mol. Biol. 138*, 149–178.

Bycroft, M., Matouschek, A., Kellis, J. T., Jr., Serrano, L., & Fersht, A. R. (1990) *Nature 346*, 488–490.

Chen, M.-J., & Mayo, K. H. (1991) *Biochemistry 30*, 6402–6411.

De Francesco, R., Pastore, A., Vecchio, G., & Cortese, R. (1991) *Biochemistry 30*, 143–147.

Deuel, T. F., Keim, P. S., Farmer, M., & Heinrikson, R. L. (1977) *Proc. Natl. Acad. Sci. U.S.A. 74*, 2256–2258.

Dolgikh, D. A., Gilmanshin, R. I., Brazhnikov, E. V., Bychkova, V. E., Semisotnov, G. V., Venyaminov, S. Y., & Ptitsyn, O. B. (1981) *FEBS Lett. 136*, 311–315.

Englander, S. W., & Poulsen, A. (1969) *Biopolymers 7*, 379–393.

Ewbank, J. L., & Creighton, T. E. (1991) *Nature 350*, 518–520.
Feng, Y., Wand, A. J., & Sligar, S. G. (1991) *Biochemistry 30*, 7711–7717.
Freire, E., Murphy, K. P., Sanchez-Ruiz, J. M., Galisteo, M. L., & Privalov, P. L. (1992) *Biochemistry 31*, 250–256.
Goldberg, M. E., Semisotnov, G. V., Friguet, B., Kuwajima, K., Ptitsyn, O. B., & Sugai, S. (1990) *FEBS Lett. 263*, 51–56.
Hermans, J., Jr. (1966) *J. Am. Chem. Soc. 88*, 2418–2425.
Holt, J. C., Harris, M. E., Holt, A., Lange, E., Henschen, A., & Niewiarowski, S. (1986) *Biochemistry 25*, 1988–1996.
Hughson, F. M., Wright, P. E., & Baldwin, R. L. (1990) *Science 249*, 1544–1548.
Jaenicke, R. (1991) *Biochemistry 30*, 3147–3161.
Jaenicke, R., & Rudolph, R. (1986) *Methods Enzymol. 131*, 218–250.
Jeener, J., Meier, B., Backman, P., & Ernst, R. R. (1979) *J. Chem. Phys. 71*, 4546–4550.
Jeng, M.-F., Englander, S. W., Elöve, G. A., Wand, A. J., & Roder, H. (1990) *Biochemistry 29*, 10433–10437.
Johnson, W. C., Jr. (1988) *Annu. Rev. Biophys. Biophys. Chem. 17*, 145–166.
Kuwajima, K. (1989) *Proteins: Struct., Funct., Genet. 6*, 87–103.
Loscalzo, J., Melnick, B., & Handin, R. I. (1985) *Arch. Biochem. Biophys. 240*, 446–455.
Lowry, O. H., Rosbough, N. J., Fan, A. L., & Randall, R. J. (1951) *J. Biol. Chem. 193*, 265–270.
Lu, J., & Dahlquist, F. W. (1992) *Biochemistry 31*, 4749–4756.
Matouschek, A., Kellis, J. T., Jr., Serrano, L., Bycroft, M., & Fersht, A. R. *Nature 356*, 440–445.
Mayo, K. H. (1991) *Biochemistry 30*, 925–934.
Mayo, K. H., & Chen, M. J. (1989) *Biochemistry 28*, 9469–9478.
Myers, J. A., Gray, G. S., Peters, D. J., Grimaila, R. J., Hunt, A. J., Maione, T. E., & Mueller, W. T. (1991) *Protein Expression Purif. 2*, 136–143.
Ohgushi, M., & Wada, A. (1983) *FEBS Lett. 164*, 21–24.
Opitz, U., Rudolph, R., Jaenicke, R., Ericsson, L., & Neurath, H. (1987) *Biochemistry 26*, 1399–1406.
Palleros, D. R., Reid, K. L., McCarty, J. S., Walker, G. C., & Fink, A. L. (1992) *J. Biol. Chem. 267*, 5279–5285.
Provencher, S. W. (1982) *Comput. Phys. Commun. 27*, 229–242.
Provencher, S. W., Glöckner, J. (1981) *Biochemistry 20*, 33–37.
Ptitsyn, O. B. (1987) *J. Protein Chem. 6*, 273–293.
Radford, S. E., Woolfson, D. N., Martin, S. R., Lowe, G., & Dobson, C. M. (1991) *Biochem. J. 273*, 211–217.
Roder, H., Elöve, G. A., & Englander, S. W. (1988) *Nature 335*, 700–704.
Ross, P. D., & Subramanian, S. (1981) *Biochemistry 20*, 3096–3102.
Rucinski, B. S., Niewiarowski, S., James, P., Walz, D. A., & Budzynski, A. Z. (1979) *Blood 53*, 47–62.
States, D. J., Haberkorn, R. A., & Ruben, D. J. (1982) *J. Magn. Reson. 48*, 286–293.
St. Charles, R., Walz, D. A., & Edwards, B. F. P. (1989) *J. Biol. Chem. 264*, 2092–2099.
Timasheff, S. N., & Inoue, H. (1968) *Biochemistry 7*, 2501–2508.
Toyo'oka, T., & Imai, K. (1984) *Anal. Chem. 56*, 2461–2464.
Udgaonkar, J. B., & Baldwin, R. L. (1988) *Nature 335*, 694–699.
Waddell, W. J. (1956) *J. Lab. Clin. Med. 48*, 311–314.
Wyman, J. (1964) *Adv. Protein Chem. 19*, 224–250.